CONTROL SYSTEM FOR INSIDE-OUT CONFIGURATION MAGNETIC BEARINGS

Gregory Buckner[1], Alan Palazzolo[2], John Kajs[3], Brian Murphy[4], Joe Beno[5]
[1] Department of Mechanical and Aerospace Engineering, North Carolina State University, Raleigh NC
[2] Department of Mechanical Engineering, Texas A&M University, College Station TX
[3,4,5] Center for Electromechanics, The University of Texas at Austin, Austin TX

ABSTRACT

The University of Texas Center for Electromechanics (UT-CEM) in association with the Texas A&M Vibration Control Lab (TAMU-VCL) has developed an active magnetic bearing control system for use in a 5 MW, 25 MJ, 20,000 RPM flywheel alternator developed under the Combat Hybrid Power Systems (CHPS) program. The inside-out topology of this flywheel (i.e., the 650 lb (294 kg) flywheel rotor is positioned outside the stator) was dictated by the extreme power density and energy density requirements, and presented unique control challenges seldom encountered in conventional magnetic bearing applications. These challenges resulted from a large number of flexible modes in the rotor and stator, requiring a high-order flexible dynamic model and extensive rotordynamic analysis. A simulation-based design effort was implemented to accomplish the primary control objective: to provide robust, efficient magnetic levitation of the CHPS rotor over a wide range of operating speeds and disturbance inputs, while minimizing the occurrence of backup bearing touchdowns. Additionally, this design effort provided critical specifications for CHPS flywheel design and component selection. Details of the CHPS magnetic bearing design, prototyping, and testing are presented in a companion paper "Inside-Out Configuration Active Magnetic Bearing Actuators".

INTRODUCTION

Researchers at the University of Texas Center for Electromechanics (UT-CEM) have been actively involved in the design, fabrication, and testing of advanced flywheel energy storage systems for several years [1,2,3,4]. One example of this research is the recently-completed Combat Hybrid Power System (CHPS) Flywheel Design Program, which developed a 5 MW, 25 MJ, 20,000 RPM flywheel alternator for military applications under DARPA funding [5]. This flywheel system was designed to power multi-MW pulse loads and provide mobility load leveling over the 15-year life cycle of a combat vehicle. The power density and energy density requirements dictated an inside-out, fully-contained flywheel topology, meaning the 650 lb (294 kg) rotor is positioned outside the stator. This unique, state-of-the-art machine consists of a vacuum housing that supports a hollow, non-rotating shaft (stator), and a magnetically-levitated composite rotor (see

Figure 1). Critical to the success of this flywheel system was the development of inside-out radial and combination magnetic bearings that could accommodate the high speeds, heavy loads, and disturbance inputs with minimal frictional losses, nominal power consumption, and modest design complexity.

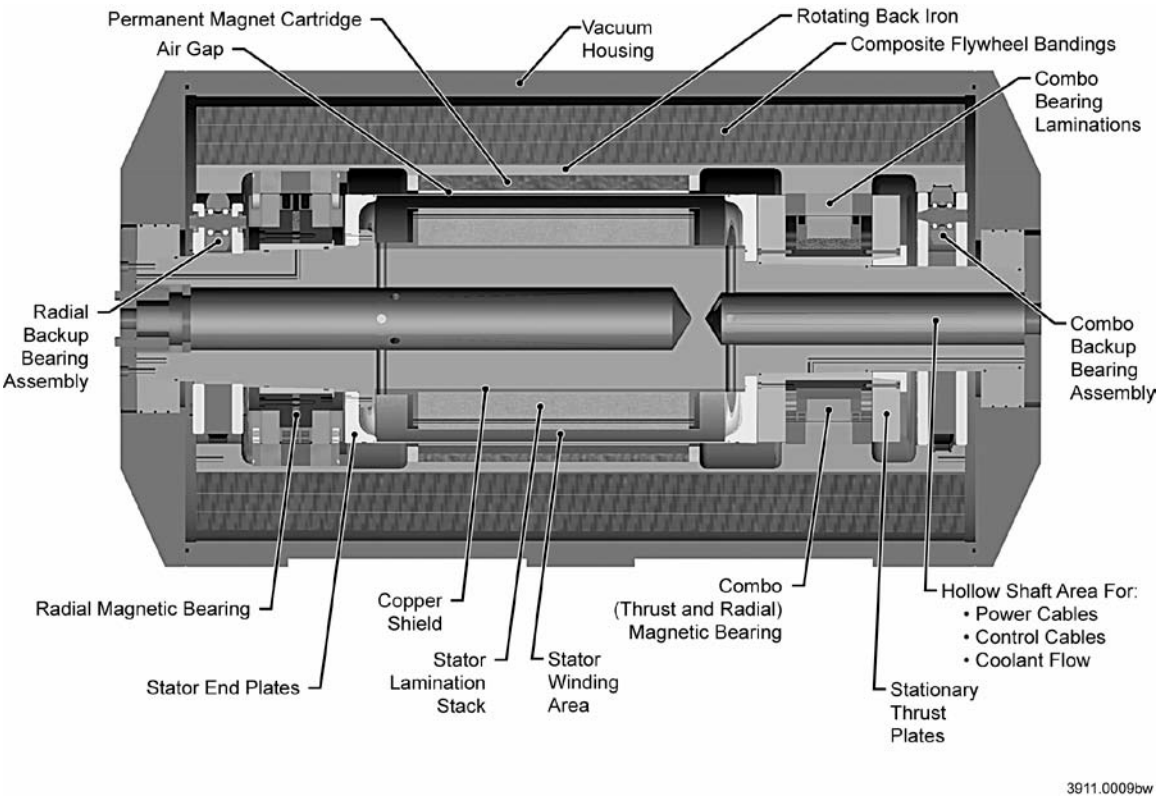

Figure 1: The UT-CEM CHPS Flywheel Design

The characteristics and capabilities of Active Magnetic Bearings (AMBs) in supporting high-speed rotors have been thoroughly documented in the literature [6,7]. For flywheel applications their most prominent features are high-speed capability, vacuum compatibility, low frictional losses, and lack of any required lubricant. Additionally, the control algorithms developed in recent years have addressed the complexities of flexible rotors and highly gyroscopic systems [8]. Modern DSP-based controllers can accommodate sophisticated control algorithms (multivariable, gain-scheduled, etc.) at high sampling rates (10-100kHz) and make magnetic bearings a viable option for demanding high-speed, flexible-rotor applications.

This paper describes a joint research effort between UT-CEM and the Texas A&M Vibration Control Laboratory (TAMU-VCL) to develop a control system for the inside-out radial magnetic bearings employed by the CHPS flywheel. The primary design objective was to provide robust, efficient magnetic levitation of the CHPS rotor over a wide range of operating speeds and disturbance inputs, while minimizing the occurrence of backup bearing touchdowns. This design effort required extensive rotordynamic analysis to determine the flywheel's critical speeds and mode shapes, and to answer

important questions that surfaced during the mechanical design of the rotor and stator, including: 1) Would passive stator damping need to be introduced? 2) Would enlarging the stator through-hole adversely affect system stability? Additionally, this controller development provided several important design specifications for the CHPS flywheel components: 1) Power amplifier selection (voltage and current requirements, wiring configurations), 2) Rotor and stator fabrication (runout and mass imbalance specifications), 3) Sensor selection (resolution and noise requirements), and 4) Digital controller selection (required processor performance, number of input/output channels, etc.).

The controller design approach followed a logical progression of steps, and relied heavily on good communication and cooperation between the two research centers. UT-CEM provided electromechanical characteristics of the bearings (inductance, resistance, current stiffness, position stiffness, etc.) and rotordynamic characteristics of the rotor, stator, and housing based on extensive Finite Element Analysis (FEA). TAMU-VCL conducted the controller design, beginning with rigid body models of the flywheel system. Later, high-order FEA models were used to study the closed-loop rotordynamic behavior, providing insight into the modal and inertial load responses. The large number of stator flexible modes, coupled with a bearing air gap that increases with speed, made the controller development particularly challenging. The final controller was optimized to provide stable operation over the entire speed range of the CHPS flywheel, and was robust to the specified levels of runout, noise, and mass imbalance.

ROTORDYNAMIC ANALYSIS

As in the case of standard rotor/stator configurations, AMB controller design is primarily concerned with critical vibration modes below the maximum operating speed (20,000 RPM, or 333 Hz for the CHPS flywheel). Additionally, modes above the operating speed can create control problems if they fall within the controller's bandwidth (3,000 Hz). For the CHPS flywheel (including the rotor, stator, and housing), there are at least 20 modes in this frequency range, thus a high-fidelity rotordynamic model was necessary for control design. To accommodate this need, a 548 degrees of freedom (DOF) model was developed at UT-CEM using TXRotor (a custom rotordynamic FEA package). This model provided a complete analysis of natural frequencies and mode shapes in the 0-3,000 Hz range, and was critical to successful controller development. Additionally, it enabled investigation of the benefits of additional stator damping in attenuating certain modes.

Figure 2 shows the CHPS rotordynamic model, a two-dimensional TXRotor finite element model made up of 3-node, cylindrically-shaped, isoparametric beam elements. Beam element models of this type are known to yield accurate estimates of lateral modes of vibration [9]. The model contains 137 nodes, 185 beam elements, and 548 DOF (4 DOF per node) — a level of detail more than adequate for this application. In addition to

the rotor (dark shaded elements), the model includes the stator through-shaft (cross-hatched elements), endplates and outer vacuum housing (light shaded elements).

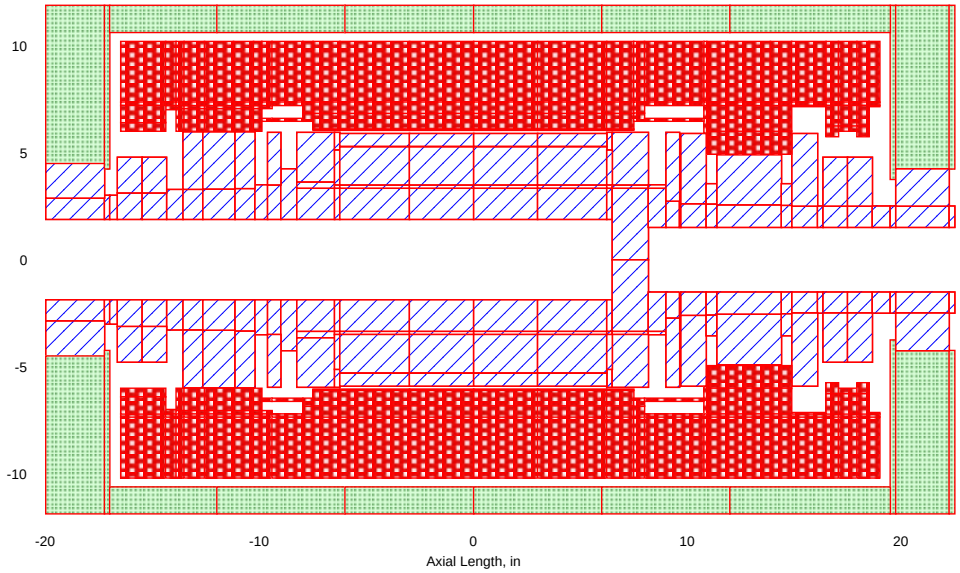

Figure 2: CHPS Rotordynamic FEA Model

The five lowest mode shapes associated with this model are shown in Figure 3. The four lowest modes occur at frequencies below the minimum operating speed of 15,000 RPM. These four modes all represent "rigid body modes", as there is no appreciable bending of either the rotor or stator. The two lowest modes are the "bouncing" and "rocking" modes, respectively, of the entire machine with the rotor and stator moving in unison. The next two higher modes are "bouncing" and "rocking" modes of the rotor, with respect to the stator. That is, the rotor is moving more than the stator. These rigid body modes must be traversed while the rotor accelerates up to its operating speed range of 15,000-20,000 RPM. The fact that these modes involve no bending of the stator or rotor means they can be easily controlled by the magnetic bearings.

The first (i.e., lowest) flexible mode of vibration (illustrated as the fifth mode shape in Figure 3) occurs at 30,000 CPM, well above the maximum operating speed of 20,000 RPM. This mode shape is the fundamental bending mode of the stator, with the rotor moving very little. A key point is that the frequency of this first flexible mode is far above the maximum rotational speed of the machine. This wide separation margin means that the mode will not interfere with AMB controller as it maintains support of the rotor in its normal operating range.

The first (i.e., lowest) flexible mode of vibration (illustrated as the fifth mode shape in Figure 3) occurs at 30,000 CPM, well above the maximum operating speed of 20,000 RPM. This mode shape is the fundamental bending mode of the stator, with the rotor moving very little. A key point is that the frequency of this first flexible mode is far above the maximum rotational speed of the machine. This wide separation margin means that the mode will not interfere with AMB controller as it maintains support of the rotor in its normal operating range.

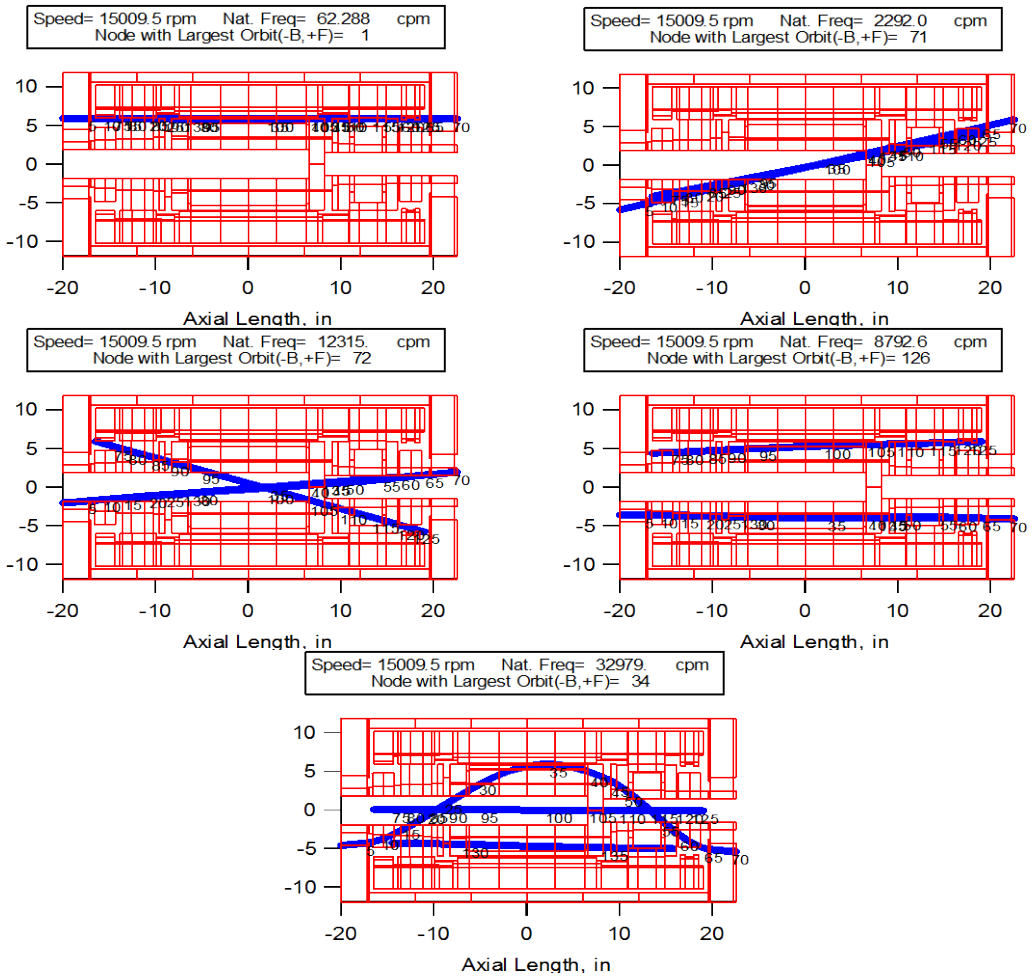

Figure 3: CHPS Rotordynamic Mode Shapes

Figure 4 is a natural frequency map, and shows that the modal frequencies actually change as the rotor speed changes. Note that the frequencies of the conical (or bounce) modes increase as speed increases. This is due to gyroscopic stiffening, which becomes stronger as the rotor spins faster. The hatched region on the plot labeled Operating Range covers the operating speed range on the horizontal axis, and on the vertical axis covers a frequency range from 20% below rotor speed to 20% above rotor speed. To avoid resonance and interference with the magnetic bearing controller while the flywheel is within its operating speed range, frequencies of all modes must lie outside this hatched region. The rigid rotor conical mode is seen to come closest to the Operating Range, but still lies outside it. More importantly, however, the first flexible mode is well removed from the Operating Range as it is well above 30,000 CPM. The results of this rotordynamic analysis indicate that the CHPS flywheel rotor is a good candidate for magnetic bearing support.

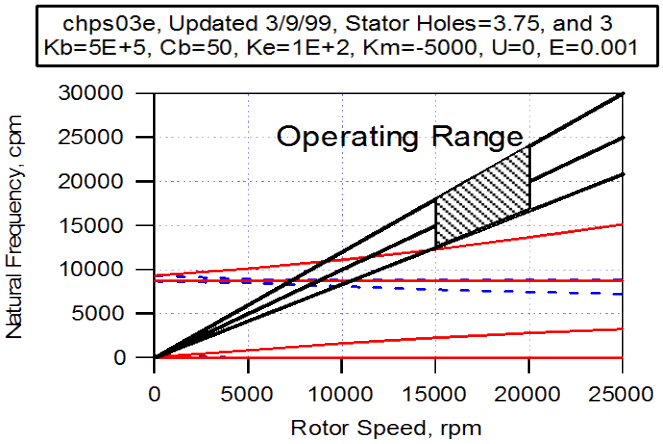

Figure 4: CHPS Natural Frequency Map

CONTROLLER DEVELOPMENT

One of the stated research objectives was to develop a straightforward AMB control system, hence controller development focused on decentralized, or Single-Input, Single-Output (SISO) approaches. In other words, the problem of controlling rotor position was simplified by assuming that radial displacements and forces at one end of the rotor were independent of displacements and forces at the other end. Additionally, displacements and forces acting in one radial direction of a bearing were independent from displacements and forces perpendicular to that direction within the same bearing. Despite the unique challenges associated with this design effort (extremely high-order rotordynamic model, large number of flexible modes, an air gap dependent on rotor speed, etc.) this design simplification has proven to be highly effective for lightly-coupled rotordynamic systems like the CHPS flywheel [6,10]. SISO development is generally more straightforward than multivariable development, requires less computational power, and provides greater flexibility when choosing a real-time processor.

Baseline PD Control

A Proportional+Derivative (PD) compensator was chosen to be the baseline controller for the CHPS flywheel. PD controllers have been selected for numerous AMB applications in the literature [6,7], primarily due to their intuitive appeal: Proportional control relates directly to bearing stiffness, while Derivative control relates to bearing damping. Independent PD controllers were selected for each measured displacement of the rotor (5 total: radial displacements at the thrust end (X and Y), radial displacements at the non-thrust end (X and Y), and thrust displacement at the thrust end (Z)). For the CHPS flywheel, each displacement sensor was co-linear with the axes of the control coils. The first step in tuning this controller was to determine a range of proportional gains (K_p) and derivative gains (K_d) that would result in stable levitation, based on the linear control system model of Figure 5. For reference purposes, a proportional gain of 16 was

determined to be equivalent to a static bearing stiffness of 88,377 lb/in (15,483,341 N/m) at the nominal operating conditions.

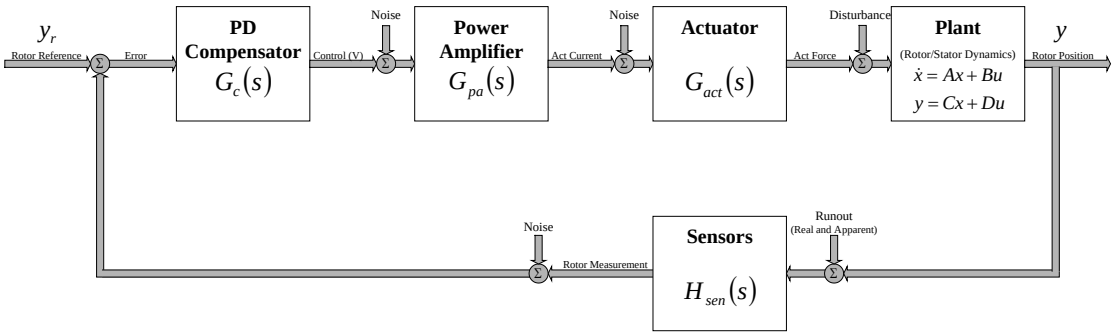

Figure 5: Linear Model of Baseline PD Control System

A linear stability analysis was conducted for a range of proportional gains ($0 \le K_p \le 80$) and derivative gains ($0 \le K_d \le 0.05$). Note that system stability also depends on controller bandwidth, as shown in Figure 6. If the bandwidth is limited to 1,000 Hz, the entire range of gains results in linear stability. If the bandwidth is increased to 2,000 Hz, all proportional gains greater than 40 destabilize the controller. For the CHPS application, a controller bandwidth of 3,000 Hz was anticipated (allowing approximately 10 control actions per rotation at full speed) resulting in a smaller range of stabilizing gains.

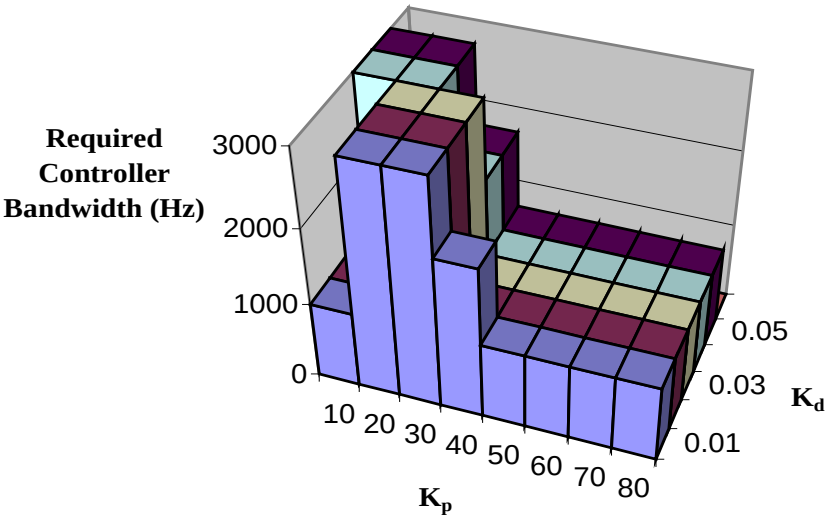

Figure 6: Linear Stability Map for Baseline PD Controller

Based on this linear stability analysis, PD controller gains were selected and controller performance was evaluated for a variety of operating conditions. Using a proportional gain of 10 and a derivative gain of 0.03, simulations confirmed AMB stability over the entire speed range (0-20,000 RPM). Figure 7 shows closed-loop orbits for one rotor

mode (top) and one stator mode (bottom) at a rotor speed of 20,000 RPM. This PD controller was robust to modest values of mass imbalance and sensor runout, but the required AMB coil voltages were excessive. At a rotor speed of 20,000 RPM, the controller required peak steady-state voltages of 50 V to compensate for a mass imbalance of 0.00001" and 150 V to compensate for a sinusoidal sensor runout of 0.0006". Clearly, controller refinements were needed to reduce this level of control effort. Furthermore, the controller was particularly sensitive to sensor noise and disturbances, indicating the need for more sophisticated control.

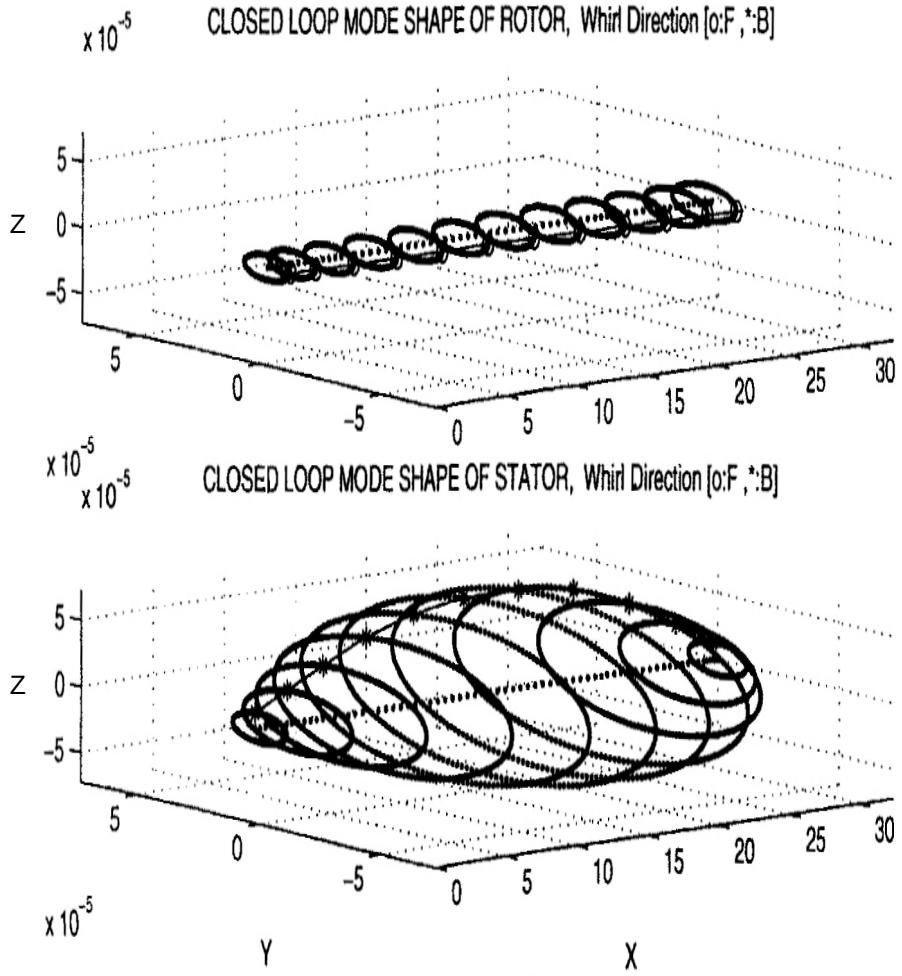

Figure 7: Closed-Loop Orbit Plots for PD Controller

Imbalance Compensation

The primary deficiency of the baseline PD controller resulted from synchronous (once per revolution) disturbances: mass imbalance and sensor runout. In each case, the controller required unacceptably high AMB coil voltages to compensate for these disturbances. To address this problem, a standard controller refinement called "imbalance compensation" was implemented [11,12]. Imbalance compensation

introduces a cascaded band-reject notch filter (whose center frequency tracks the rotor speed) to attenuate controller responses to synchronous disturbances. In other words, mass imbalance and synchronous runout are not controlled, which enables the rotor to spin about its inertial axis (instead of controlling it to spin about is geometric axis). Assuming adequate air gap exists, the rotor no longer transmits imbalance forces to the stator/housing (vibration and noise are reduced), and synchronous control effort is virtually eliminated.

Figure 8 illustrates the dramatic reductions in control effort achieved by introducing a tracking notch filter. Figure 8.a shows the peak coil voltages (which depend on rotor speed) required to compensate for a mass imbalance of 0.00001", with the notch filter fixed at 20,000 CPM. As the rotor speed approaches the filter's center frequency (20,000 RPM), the required coil voltage drops to nearly zero. Figure 8.b shows a time response of the required coil voltage, at a rotor speed of 20,000 RPM, as the fixed notch filter is inserted. For times 0<=t<=0.1 seconds, the controller requires a peak voltage of 50 V to compensate for the imbalance. As the notch filter is inserted (at time t=0.1 seconds), the controller effort is dramatically reduced.

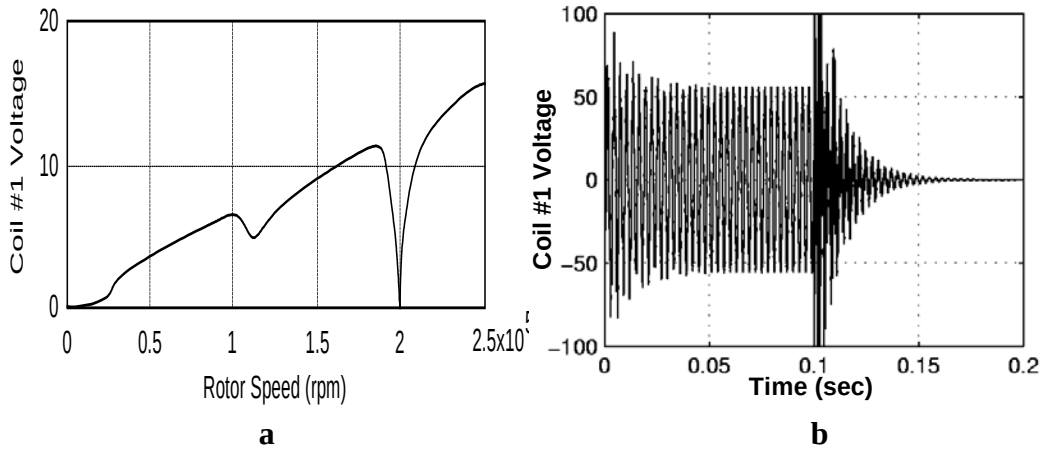

Figure 8: Coil Voltage Requirements for 20 kHz Imbalance Compensation: a) Steady-State Peak Voltages b) Transient Voltage During Notch Introduction

Fixed-Frequency Notch Filtering

Although the introduction of a tracking notch filter significantly reduced the control effort and improved robustness to mass imbalance and synchronous runout, it had an undesirable impact on overall system stability. Certain high-frequency modes between 2,500 Hz and 3,000 Hz (within the controller bandwidth) became very poorly damped or even unstable as a result of this refinement. Some of these modes were associated with low stator damping, and prompted a rotordynamic analysis to investigate the benefits of adding passive stator damping. This analysis concluded no significant benefits could be achieved with increased damping, so additional controller refinements were needed.

To counteract these unstable modes, a series of fixed-frequency notch filters and a lead compensator were systematically cascaded with the existing controller, as shown in Figure 9. The resulting cascaded controller demonstrated acceptable performance over the operating range for a larger range of disturbances and noise.

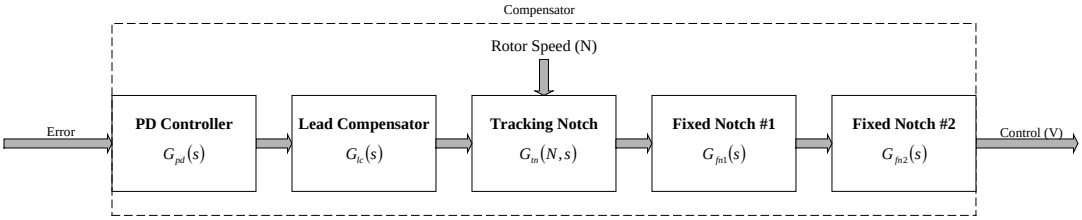

Figure 9: Final Cascaded Bearing Controller

CONTROL SYSTEM PERFORMANCE EVALUATION

An extensive series of dynamic simulations was conducted to assess system performance for a variety of operating conditions and disturbance inputs. Although the design effort relied on linear models of control system components (Figure 5) and simplified models of sensor runout, these final evaluations included realistic models of system nonlinearities and experimental runout data. The most significant nonlinearities were voltage and current limitations associated with the power amplifiers and AMB stiffness variations (position and current stiffness) associated with rotor speed (due to changes in the air gap with rotor speed). Because sensor runout was identified as being critical to overall system performance, UT-CEM fabricated an experimental test-rig to collect representative runout data using the same optical sensor hardware and unpolished materials planned for the CHPS Flywheel. This runout data, presented in Figure 10, provided authentic, "worst-case" disturbance information for control system evaluation.

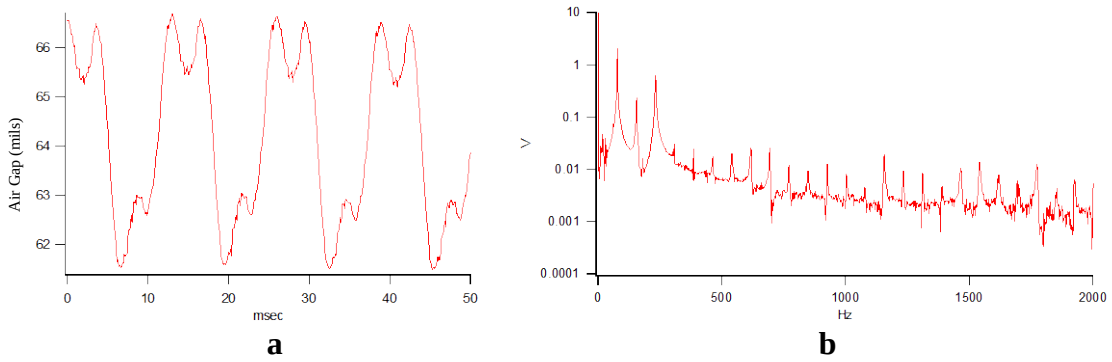

Figure 10: Experimental Air Gap Measurments for the CHPS Flywheel: a) Optical Sensor Time Series b) Unfiltered FFT Showing Harmonic Content

The simulations confirmed the control system's effectiveness with respect to the design objectives. Most importantly, this cascaded design maintained stable levitation of the CHPS rotor over the entire speed range (0-20,000 RPM) for a variety of disturbance inputs, including authentic sensor runout, mass imbalance, sensor noise, and inertial loading (due to vehicle cornering and braking). Additionally, the peak coil voltages were within the design specifications for this system (150 V) and currents were within the specified limits for the selected power amplifiers, with adequate margin against clipping. Margin against saturation in the flux path circuit was also achieved. Finally, these simulations provided valuable design specifications for the power amplifiers, sensors, and machining tolerances.

CONCLUSIONS

Researchers from UT-CEM and TAMU-VCL have successfully developed a control system for the inside-out radial magnetic bearings employed by the CHPS flywheel. Although the SISO cascaded control architecture is straightforward, this controller conquered numerous design challenges (extremely large number of system states, lightly-damped flexible modes, air gap dependent on rotor speed, etc.) to meet or exceed each of the design objectives. Moreover, this design effort is the first known application of AMBs to inside-out configuration bearings. Extensive performance simulations confirmed that the control system provides robust, efficient magnetic levitation of the CHPS rotor over a wide range of operating speeds and disturbance inputs, while minimizing the occurrence of backup bearing touchdowns. Additionally, this design effort provided critical design specifications for CHPS flywheel design and component selection.

REFERENCES

1. R. Hayes, J. Kajs, R. Thompson, J. Beno, "Design and Testing of a Flywheel Battery for a Transit Bus", 1999 SAE International Congress and Exposition, March 1-4, 1999, Detroit, MI.

2. R. Thompson, R. Hayes, J. Beno, "The Flywheel Battery Containment Problem-Light Weight Solution", 1999 SAE International Congress and Exposition, March 1-4, 1999, Detroit, MI.

3. B. Murphy, J. Beno, D. Bresie, "Bearing Loads in a Vehicular Flywheel Battery", 1997 SAE International Congress and Exposition, Feb 24-27, 1997, Detroit, MI.

4. M. Pichot, J. Kramer, R. Hayes, R.C. Thompson, J. Beno, "The Flywheel Battery Containment Problem", 1997 SAE International Congress and Exposition, Feb 24-27, 1997, Detroit, MI.

5. M. Pichot, J. Kajs, A. Ouroua, J. Beno, R. Hayes, “Inside-Out Configuration Active Magnetic Bearing Actuators”, 5th International Symposium on Magnetic Suspension Technology, 1999.

6. G. Schweitzer, H. Bleuler, A. Traxler, Active Magnetic Bearings: Basics, Properties and Applications of Active Magnetic Bearings, vdf Hochschulverlag AG, 1994.

7. R. Siegwart, R. Larsonneur, and A. Traxler, “Design and Performance of a High Speed Milling Spindle in Digitially Controlled Active Magnetic Bearings”, Proceedings of 2nd International Symposium on Magnetic Bearings, Tokyo, 1990.

8. M. Ahrens, L. Kucera, and R. Larsonneur, “mu-Synthesis of Flexible Rotor-Magnetic Bearing Systems”, IEEE Transactions on Control Systems Technology, Vol. 4, No. 5, September 1996.

9. J. M. Vance, Rotordynamics of Turbomachinery, John Wiley & Sons, 1998.

10. H. Bleuler, “Decentralized Control of Magnetic Bearing Systems”, Dissertation, Eidgenössische Technische Hochschule, Zürich, 1984 (Diss. ETH Nr. 7573).

11. R. Herzog, B. Philipp, G. Conrad, L. Rene, “Unbalance Compensation Using Generalized Notch Filters in the Multivariable Feedback of Magnetic Bearings”, IEEE Transactions on Control Systems Technology, Vol. 4, No. 5, pp. 580-586, September 1996.

12. Knospe, C.R., “Stability and Performance of Notch Filter Controllers for Unbalance Response”, Proceedings of the International Symposium on Magnetic Suspension Technology, NASA Langley Research Center, Hampton VA 1991.